Sports Eng (2010) 12:123–133
DOI 10.1007/s12283-010-0038-z

ORIGINAL ARTICLE

Finite element simulation of the ski–snow interaction of an alpine ski in a carved turn

Peter Federolf · Markus Roos · Anton Lüthi · Jürg Dual

Published online: 31 March 2010

Abstract Skiing manufacturers depend on the development of new skis on trial and error cycles and extensive product testing. Simulation tools, such as the finite element method, might be able to reduce the number of required testing cycles. However, computer programs simulating a ski in the situation of a turn so far lack realistic ski–snow interaction models. The aim of this study was to (a) implement a finite element simulation of a ski in a carved turn with an experimentally validated ski–snow interaction model, and (b) comparison of the simulation results with instantaneous turn radii determined for an actual carved turn. A quasi-static approach was chosen in which the ski–snow interaction was implemented as a boundary condition on the running surface of the ski. A stepwise linear function was used to characterise the snow pressure resisting the penetration of the ski. In a carved turn the rear section of the ski interacts with the groove that forms in the snow. Two effects were incorporated in the simulation to model this situation: (a) the plasticity of the snow deformation, (b) the influence of the ski's side-cut on the formation and shape of this groove. The simulation results agreed well with experiments characterising snow penetration. Implementation of the groove in the ski–snow interaction model allowed calculation of the instantaneous turn radii measured in actual turns, but also caused significant numerical instability. The simulation contributes to the understanding of the mechanical aspects of the ski–snow interaction in carved turns and can be used to evaluate new ski designs.

Keywords FEM · Alpine skiing · Snow mechanics · Sports engineering

P. Federolf (✉)
Human Performance Laboratory, University of Calgary, Calgary, Canada
e-mail: peter.federolf@kin.ucalgary.ca

M. Roos
Institute of Computational Physics, Zurich University of Applied Sciences, Winterthur, Switzerland

P. Federolf · A. Lüthi
WSL Institute for Snow and Avalanche Research SLF, Davos, Switzerland

J. Dual
Institute of Mechanical Systems, Swiss Federal Institute of Technology, Zurich, Switzerland

1 Introduction

Alpine skiing is one of the most popular winter sports and alpine ski manufacturers achieve millions in annual turnover. However, despite its huge economical importance, skiing manufacturers still depend on the development of new ski types on trial and error cycles that require extensive product testing. Other manufacturing industries employ sophisticated computer simulation methods, such as the finite element modelling (FEM), to reduce the number of expensive and time-consuming testing cycles required in their product development. A FEM simulation of skis in the situation of a turn is difficult to implement because (a) skis are sandwich structures consisting of several isotropic and non-isotropic material layers the mechanical properties of which are often not well known, and (b) the ski–snow interaction in skiing is a complicated combination of different mechanical processes, in particular, bending and torsion of the ski [1–3], penetration of the snow [4–6], machining of snow [7–9], friction [10–14], and system vibrations [15, 16]. Computer simulation

programs that have been developed in recent years [6, 17–26] focus on the calculation of the deformation of the ski in order to predict performance variables, such as the ski radius or the pressure distribution on the running surface of the ski. A limitation of most of these simulation approaches is a severe simplification of the ski–snow interaction processes. To our knowledge there are only two simulation approaches that incorporate the plasticity of the snow deformation [27, 28]. Only a small number of the simulation methods described in the literature have been validated and none with data from an actual carved turn executed by a skier.

The aim of the current work was the development of a simulation model of a ski in the state of a carved turn using the finite element method. The simulation is intended to be used on the one hand to assist in the development of new ski and binding designs and on the other hand to allow a systematic analysis of turn parameters and their interrelationship. The output of the simulation should particularly include the deformed shape of the ski. The ski's shape determines its turn radius which will be compared to the instantaneous turn radius measured in an actual carved turn. The purpose of this paper is to describe the FE model, its boundary conditions, the experimental validation procedures, and to discuss the model's advantages and limitations. Application of the simulation described here in a parameter study investigating the influence of the input variables edging angle, force on the binding, and snow conditions will be presented in a subsequent publication.

2 Methods

2.1 Selected ski and binding models

Two skis were selected for this study: the all-round carver ski *Stöckli Spirit* of the winter season 2001/2002 and the race carver *Stöckli Laser GS* of season 2001/2002. Present day skis are laminates of several material layers. For each ski the manufacturer *Stöckli Swiss Sports AG*., Wolhusen, Switzerland provided detailed data of construction and geometry.

The binding model selected for this study was the *Rave Powerride* binding of season 2001 manufactured by *Fritschi AG. Swiss Bindings*, Reichenbach/Kandertal, Switzerland. This binding offers a high stance height of the ski boot rendering an additional damping plate unnecessary. In this binding the heel clamps and the release mechanism are mounted on a stiff aluminium beam, which is connected to the toe part with a hinge joint. If the ski is bent, the beam can slide freely back and forth on a rail incorporated on the heel part of the binding.

2.2 Finite element model

Ski and binding were modelled using the commercial FEM-software package *SESES*^{TM} (*Numerical Modelling GmbH.*, Winterthur, Switzerland). The binding was represented using 8-node volume elements, while the ski was represented using shell elements. The governing equations of the *SESES*^{TM} shell elements are based on the classical Kirchhoff plate theory [29]. SESES^{TM} uses the so-called free formulation shell elements [30] to calculate the element stiffness matrices. The geometry of the shell is specified in three dimensions in SESES^{TM}. Since the ski consists of several layers, SESES^{TM} calculates the corresponding compound bending and stretching elasticity matrix from the given 3D-elasticity tensors C_{ijkl} [29] by suitable integrals along the transverse direction.

For a ski represented by such shell elements, bending and in-plane stretching deformations are calculated accurately. However, the neglect of transverse shear in the classical Kirchhoff plate theory causes the FEM model of the ski to have a higher torsional stiffness than in reality. Despite this disadvantage, shell elements were selected because they allowed the number of degrees of freedom of the model to be reduced and kept calculation times to a reasonable level.

2.3 Discretisation and material properties of the ski

Each material layer of the ski was represented by a one-element layer. Between the layers an adhesive layer with a thickness of 0.2 mm [31] was included. The element discretisation along the ski axis was chosen such that the elements had a length between 50 and 80 mm. This length scale of the discretisation allowed reasonable calculation times and it was verified that the numerical solution was independent of element length for values smaller than 150 mm. The width of the elements was of the order of 1–2 mm near the ski edge and 4–5 mm near the centre of the ski. A higher element density was chosen near the ski edge to provide a better resolution of the pressure distribution calculated at the ski–snow contact.

Many component materials are isotropic. In this case, Young's modulus and the Poisson ratio are sufficient to express the stiffness tensor C_{ijkl}. Young's modulus and the Poisson ratio of most component materials were either taken from standard literature or provided by the ski company Stöckli (they are considered proprietary and cannot be published here). The mechanical properties of the thin adhesive layers and the Poisson ratio of some other materials were estimated. The wood core and the fibre glass composite layers within the ski are non-isotropic materials for which the most important components of the C_{ijkl} tensor were determined in tensile tests [31].

Comprehensive parameter studies and validation experiments were conducted to ensure that the employed shell elements could predict the deformation of the ski. Maximal deviations between experimental and numerical results were 15% in bending tests and 20% in torsion tests. However, some of these deviations can be attributed to an idealisation of the adopted boundary conditions. The parameter studies also confirmed that the bending stiffness of the ski's sandwich structure is mainly determined by the stiffness and thickness of the metal layers and the thickness of the wood core, the contribution of the other materials to the overall stiffness properties was marginal.

2.4 Implementation of the ski binding

Modern bindings are complicated mechanical devices, which comprise a large number of different component parts. However, for a calculation of the turn radius and the pressure at the ski snow interface only the influence of the binding on the system stiffness and the force transfer onto the ski are relevant. Therefore, the binding was modelled as three separate finite element blocks representing (a) the beam carrying the holding clamps and the release mechanism for the ski boot, (b) the front plate, and (c) the rear plate, which are screwed onto the ski. The mechanical functionality of the binding was represented in the model by defining internal constraints at the joint, the rail, the screws between binding and ski, and at all other contacting surfaces that transfer pressure or forces. Internal friction between parts of the binding was neglected. The material properties of the two blocks directly attached to the ski were adjusted such that the calculated bending stiffness of the whole ski-binding system agreed with experimental results obtained from three point bending tests.

2.5 Boundary conditions

The main external forces acting on the ski-binding system during a turn are the forces at the binding, the pressure at the ski–snow interface, and gravity. In the simulation a quasi-static approach was chosen. According to D'Alembert's principle, system accelerations were expressed as inertial forces in the reference system of the ski and equated with the external forces acting on the system:

$$F_{\text{athlete}}(t) + F_{\text{SSI}}(\text{t}) + G_{\text{ski}}(t) + F_{\text{inertia}}(t) = 0 \quad (1)$$

$$M_{\text{athlete}}(t) + M_{\text{SSI}}(t) + M_{\text{Gski}}(t) + M_{\text{inertia}}(t) = 0 \quad (2)$$

where $F_{\text{athlete}}(t)$ and $M_{\text{athlete}}(t)$ are the forces and moments transferred from the athlete onto the binding, $F_{\text{SSI}}(t)$ and $M_{\text{SSI}}(t)$ are the forces and moments created by ski–snow interaction, $G_{\text{ski}}(t)$ and $M_{\text{Gski}}(t)$ are the forces and moments caused by gravitation, and $F_{\text{inertia}}(t)$ and $M_{\text{inertia}}(t)$ are inertial forces and moments acting on the ski. In this study the centre of the ski boot at the upper surface of the ski was chosen as reference point for the moment calculations. Other forces on the system, e.g. air resistance, were neglected.

The forces $F_{\text{athlete}}(t)$ and moments $M_{\text{athlete}}(t)$ acting on the binding were determined experimentally (see Sect. 3) and defined on the appropriate surface area $\partial\Omega$ of the binding by prescribing the external force components F_{l} (using Einstein convention for the notation):

$$(F_{\text{ext}})_l = \int_{\partial\Omega} n_k s_{lk} \mathrm{d}A \quad (3)$$

where n is the normal vector on the surface $\partial\Omega$, s is the stress tensor, and k and l are indices.

The gravitational forces $G_{\text{ski}}(t)$ and inertial forces $F_{\text{inertia}}(t)$ can be obtained from kinematic measurements that determined the position and orientation of the ski in an external reference frame as a function of time. These were implemented as volumetric forces assigned to each element depending on its density. Hence, the associated moments created by these forces were generated automatically and did not have to be specified explicitly. Terms due to relative accelerations of parts of the ski-binding system with respect to its centre of mass were neglected based on an analysis of the inertial components created by the rotating reference system of the ski [27] and based on the assumptions that no significant vibrations are present.

At the ski–snow interface two types of forces are created: reaction forces due to the penetration of the ski into the snow and frictional forces. In the simulation, frictional forces were neglected, i.e. it was assumed that the resistive forces always act normal to the ski's running surface. The reaction force $F_{\text{SSI}}(t)$ exerted by the snow to the penetrating ski was implemented as a "generalised Neumann" boundary condition on the whole running surface by prescribing the external force component $(F_{\text{ext}})_l$ on the boundary surface $\partial\Omega$ as a function $f(u_{\text{l}})$ of the displacement u_{l} (k and l being indices):

$$(F_{\text{ext}})_l = \int_{\partial\Omega} n_{\text{k}} s_{\text{lk}} \mathrm{d}A = f(u_{\text{l}}) \quad (4)$$

The function $f(u_{\text{l}})$ depends on the penetration depth D of the ski into the snow and on the snow strength. The coordinate system for the simulation was chosen such that the snow surface coincides with the x–y-plane. Thus, the penetration depth D of any point of the ski model could easily be determined from the z-coordinate of the (local) displacement.

2.6 Ski–snow contact in a static situation

The average reaction pressure p_{average} that the snow exerts to a penetrating plate can over a wide range of snow types

be appropriately described by a piecewise linear function of the penetration depth D [32]:

$$p_{\text{average}}(D) = \begin{cases} A(\theta) \cdot D + B & D > 0 \\ 0 & D \leq 0 \end{cases} \quad (5)$$

The coefficients A and B define the snow strength and A depends on the edging angle θ of the penetrating plate. For groomed snow on ski slopes the coefficient A is in the range 5–40 kPa/mm for $\theta < 40°$ or in the range 2–20 kPa/mm for $\theta > 40°$. B is in the range between 0 and 400 kPa [32]. The penetration into the snow is facilitated by fracture processes within the snow. Deviations from Eq. 5 may occur due to random nature of these fracture events. Such deviations were particularly observed for large edging angles of the ski.

The simulation requires the actual pressure $p_{\text{Snow}}(D)$ at a given point P of the boundary surface:

$$p_{\text{Snow}}(D) = \begin{cases} 2A \cdot D + B & D > 0 \\ 0 & D \leq 0 \end{cases} \quad (6)$$

as can be derived from Eq. 10 by using the definition of the averaged pressure on the plate:

$$p_{\text{average}}(D) = \frac{\int_0^D p_{\text{Snow}}(D')\, \mathrm{d}D'}{D} = AD + B. \quad (7)$$

The function $p_{\text{Snow}}(D)$ contains a non-differentiable point at the transition from positive penetration depths $D > 0$ to negative penetration depths $D < 0$ which would cause numeric divergence of the simulation. Therefore, this function was approximated with a smoothing function:

$$p_{\text{Snow}}(D) = 2A \cdot \text{ramp}(D) + B \cdot \text{step}(D) \quad (8)$$

Using

$$\begin{aligned} \text{step}(D) &= \frac{1}{2} \cdot \left(1 + \tanh\left(\frac{D - D_{\text{off}}}{\varepsilon_{\text{Step}}}\right)\right) \\ \text{ramp}(D) &= \frac{1}{2}\left(\sqrt{(D - D_{\text{off}})^2 + \varepsilon_{\text{Ramp}}^2} + (D - D_{\text{off}})\right) \end{aligned} \quad (9)$$

where D_{off} is an offset and the coefficients $\varepsilon_{\text{Step}}$ and $\varepsilon_{\text{Ramp}}$ determine the width of the transition between the two nearly linear parts of the functions. In the simulation $\varepsilon_{\text{Step}}$ and $\varepsilon_{\text{Ramp}}$ were chosen to be smaller than 0.5 mm creating a transition zone of approximately ±1 mm depth. Considering that the typical grain size of the snow on groomed ski slopes is in the range of 1–3 mm this transition zone seemed acceptable.

2.7 Solving algorithm in a static situation

The generalised Neumann boundary conditions for the ski–snow interaction provide a non-linearity as the reaction force depends on the penetration depth, i.e. the local displacement. An iterative solution procedure is therefore mandatory. The implemented algorithm iteratively finds the deformation state of the ski and the corresponding distribution of snow pressure such that the quasi-static Eqs. 5 and 6 are satisfied. The iteration usually converged to a stable solution in less than 10 calculation steps, however, the calculation procedure is very sensitive to the initial conditions and may not converge at all if not properly initialised. The linearised system matrix is non-symmetric and was solved iteratively by a stabilised biconjugate gradient solver [29].

2.8 Ski–snow contact for a ski in motion

The definition of a carving turn in alpine skiing is that the rear section of the ski glides in the groove formed by the front section. The validation measurements conducted in this study showed that it is essential to understand how the groove is formed and how it affects the deformation of the ski. Two phenomena have to be considered and incorporated into the model:

(a) The plasticity of the snow deformation, i.e. formation of a groove in the snow.
(b) The "side-cut effect", i.e. how the ski's side-cut affects the shape of the groove.

2.8.1 *Plasticity of the snow deformation*

As the ski shovel passes over the snow the pressure increases until a maximum pressure is reached somewhere in the middle of the ski. As long as the pressure increases, the ski penetrates deeper into the snow. However, once the point of maximum pressure has passed, the snow is effectively unloaded, i.e. the ski does not penetrate deeper, but remains on the surface of the groove that has formed already.

To implement the plastic deformation behaviour of the snow, a second, superposed iteration loop was adopted. In the first iteration step, the point on the ski–snow contact area with maximum pressure $p_{\max}$ and the maximal penetration depth $D_{\max}$ were determined using the snow penetration function (Eq. 12) to calculate the snow pressure. In the following iteration steps, the boundary area was split into a loading area (shovel to point of maximum pressure) and an unloading area (point of maximum pressure to ski end). In the unloading area, the function describing the snow resistance pressure was replaced by a function describing unloading of snow:

$$P_{\text{unload}}(D) = \begin{cases} C \cdot (D - D_{\max}) + p_{\max} & D_{\max} \geq D > D_0 \\ 0 & D \leq D_0 \end{cases} \quad (10)$$

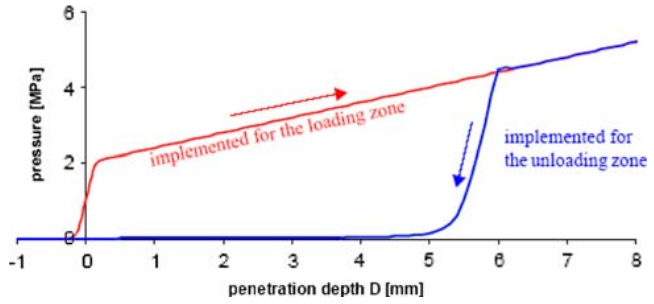

Fig. 1 Example of the mathematical functions implemented to calculate the resistive snow pressure in case of loading (*upper curve*) and unloading (*lower curve*) with arbitrarily chosen coefficients $A = 0.4$ MPa/mm, $B = 2$ MPa, $C = 8$ MPa/mm, $D_{max} = 6$ mm

Coefficient C in this equation depends on residual elastic energy in the snow and is typically in the range 0.15–1.15 MPa/mm [27]. Only the global maximum in the snow pressure was considered in the current implementation. Local maxima that may occur close to the ski tip in case of small edging angles were not considered. For better numerical stability the function actually used was a differentiable approximation that converged to the loading function if the pressure in a later iteration step should exceed the maximum pressure determined in the previous iteration step (Fig. 1).

2.8.2 The "side-cut effect"

In 2000, Howe presented a model to approximate the shape of the lower ski edge with and without snow penetration [3]. If a ski is set on its edge and pushed into the snow, then the side-cut of the ski determines the contact line between ski and snow (Fig. 2). On a hard, icy surface this contact line can be used to approximate the turn radius R_{Howe}. On a snow surface the ski penetrates the snow at this contact line to the depth at which the snow's resistive pressure is equal to the load exerted by the ski onto the snow. At the ski centre this pressure is maximal and therefore the ski penetrates deepest at the ski centre. At the ski shovel and at the ski end the pressure on the snow is small and therefore ski shovel and ski end do not penetrate the snow [3]. As the ski penetrates the snow in the ski centre it becomes more bent and the turn radius $R_{Howe,snow}$ becomes smaller.

However, Howe's model does not take into account that in an ideally carved turn the rear section of the ski glides in the groove that has formed in the snow and thus the actual turn radius depends on the curvature of the groove that forms, not on the curvature of the entire ski edge. The width of the groove that forms in the snow as a ski passes over a point on the snow surface depends on the one hand on the snow penetration and on the other hand on the

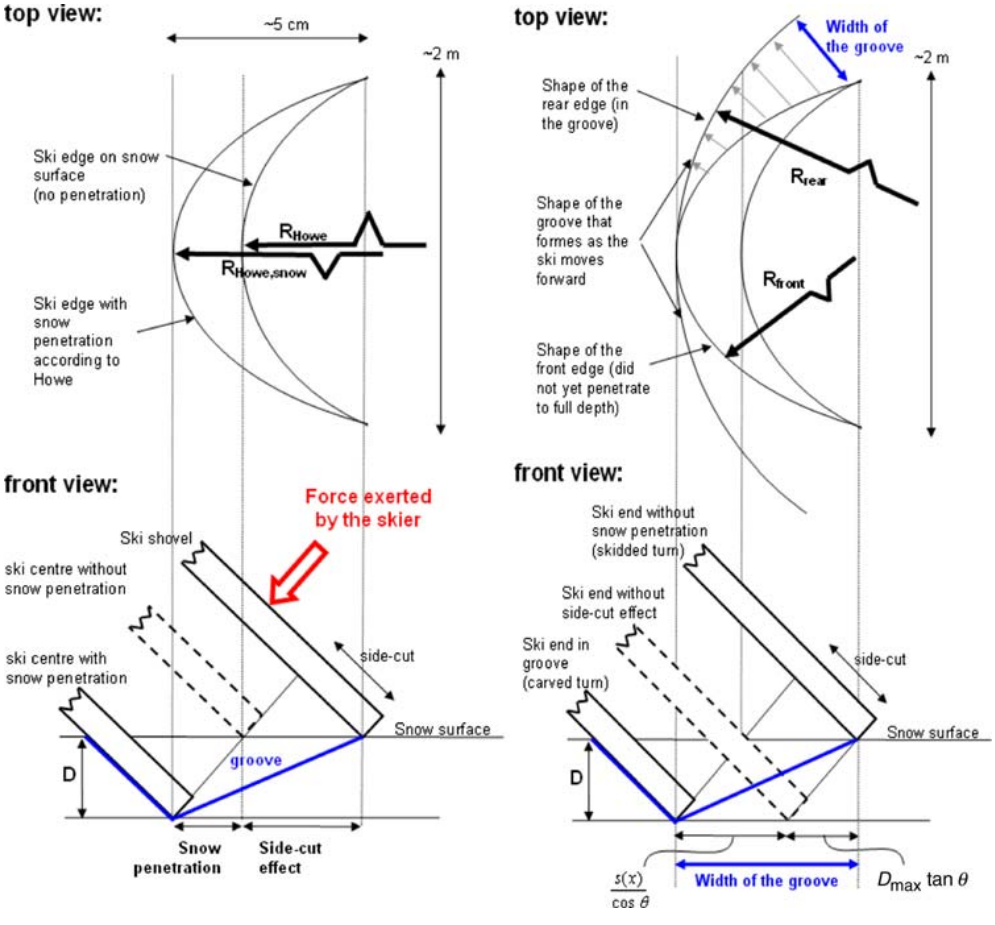

Fig. 2 *Top view* the shape of an edged and bent ski (in the situation of a turn) indicated as the position of the lower ski edge that penetrates the snow and determines the turn radius. *Front view* cross section of the ski at the ski shovel (on the snow surface) and at the ski centre (which penetrates the snow). As the ski moves forward and penetrates deeper into the snow, the snow above the *thick line* is removed, i.e. the *thick line* indicates the groove that forms in the snow. *Left* determination of the turn radius according to Howe [3]. *Right* side-cut effect: the rear section of ski end does not return to the snow surface (as in Howe's model) but remains in the groove that has formed

side-cut of the ski: consider the front view in Fig. 2: as the ski moves forward all snow above the thick line is removed. The groove that forms in the snow therefore does not have a 90° angle but a much wider angle, which agrees well with observations in the field. In a static case (Howe's model) or when the ski is skidding, then the ski edge at the rear section returns to the snow surface and the groove has a 90° angle. If the ski is carving, then the rear section of the ski glides within the groove and therefore the curvature of the ski is reduced in the rear section compared with that of the front section. The radius R_{rear} determined from the rear section of the ski edge (projected to the snow surface) is the best approximation of the actual turn radius, which can be determined from the trace remaining in the snow after a carved turn. The ski's front section has a different curvature which can be approximated with Howe's model ($R_{\text{front}} \approx R_{\text{Howe,snow}}$).

If a steady state is assumed and the ski is loaded at the ski centre without significant forward or backward leaning, then a symmetrical shape of the groove can be assumed and the position of the rear ski edge can be approximated (Fig. 2).

In the simulation this is implemented by

(a) defining the plastic snow model (which leads to the theoretical position of the ski end with a correct penetration depth but a wrong lateral position as indicated by the dashed line in Fig. 2), and
(b) modifying the boundary condition on the rear part of the ski such that snow resistance pressure is only present after a lateral displacement of the ski by $L(x)$. The length $L(x)$ represents the width of the groove parallel to the snow surface. In the simulation $L(x)$ can be calculated from the penetration depth D_{max}, the side-cut $s(x)$, and the edging angle θ:

$$L(x) = D_{\text{max}} \tan\theta + \frac{s(x)}{\cos\theta} \tag{11}$$

Here x is the position along the ski length. The side-cut $s(x)$ at position x can be calculated from the ski's width $W(x)$ at position x, the width W_S at the shovel and the width W_E at the ski end:

$$s(x) = \frac{1}{2}\left(\frac{W_S + W_E}{2} - W(x)\right) \tag{12}$$

2.9 Solving algorithm for a ski in motion

The final shape of the ski is determined in an iterative process starting from a solution for a static state. In the following iteration steps a new equilibrium state is determined for which the boundary condition at the ski–snow interface includes the plastic snow model and the side-cut effect. These modifications of the ski–snow boundary conditions cause the ski to rotate slightly, such that its rear section rests in the groove and is less bent than in the static situation (Fig. 3). A number of additional requirements limit the applicability of this solution, namely the assumption of a steady state and loading that causes a symmetrical ski deformation. In the case of significant moments acting on the binding, e.g. caused by forward or backward leaning of the skier, the solution is not valid. A second limitation of this implementation is the severely decreased numerical stability: the simulation converges only for a limited range of input parameters to a stable solution. Particularly for large edging angles ($\theta > 70°$) the model cannot be solved.

3 Experimental validation procedures

The validation of the simulation results was carried out in three steps: first, the implemented snow model was validated by measuring the snow resistive force on a penetrating plate and simulating the same situation using the snow model as a boundary condition (Fig. 4). In both cases the force was incrementally increased and the penetration depth into the snow was determined. The experiment and the simulation were repeated twice for the following edging angles: 20, 30, 40, 45, 55, and 60°.

As a second validation step, the shape of the ski was calculated for a static loading case and compared to the shape determined in a static experiment (Fig. 5). To compare the shape, the position of the lower ski edge was determined in the simulation and compared with the shape of the groove created on an even snow surface when a ski was pressed into the snow with a force of 3,000 N. The position of the groove was measured at 16 positions along ski with a distance of 10 cm between each measurement. The accuracy of the measured position was approximately ±3 mm. Even though the snow on the experimental field seemed very homogeneous, several large clods of snow broke loose during the experiment (Fig. 5). This caused some deviation in the curvature of the ski edge. The experiment was conducted at edging angles of 39° and 53°.

The third validation step was to compare the ski shape calculated in the simulation with the shape determined for an actual carved turn. All input parameters necessary for the simulation, particularly the load on the ski and the edging angle, were measured in an actual carved turn skied by an experienced ski racer. The experiment was carried out in a ski dome in Neuss, Germany on a section with constant slope. The skier was equipped with two dynamometers (Kistler, Winterthur, Switzerland) mounted between ski and binding to record 3D-forces and 3D-moments acting on the skis. Several carving turns were skied between gates defining the path while the skier's

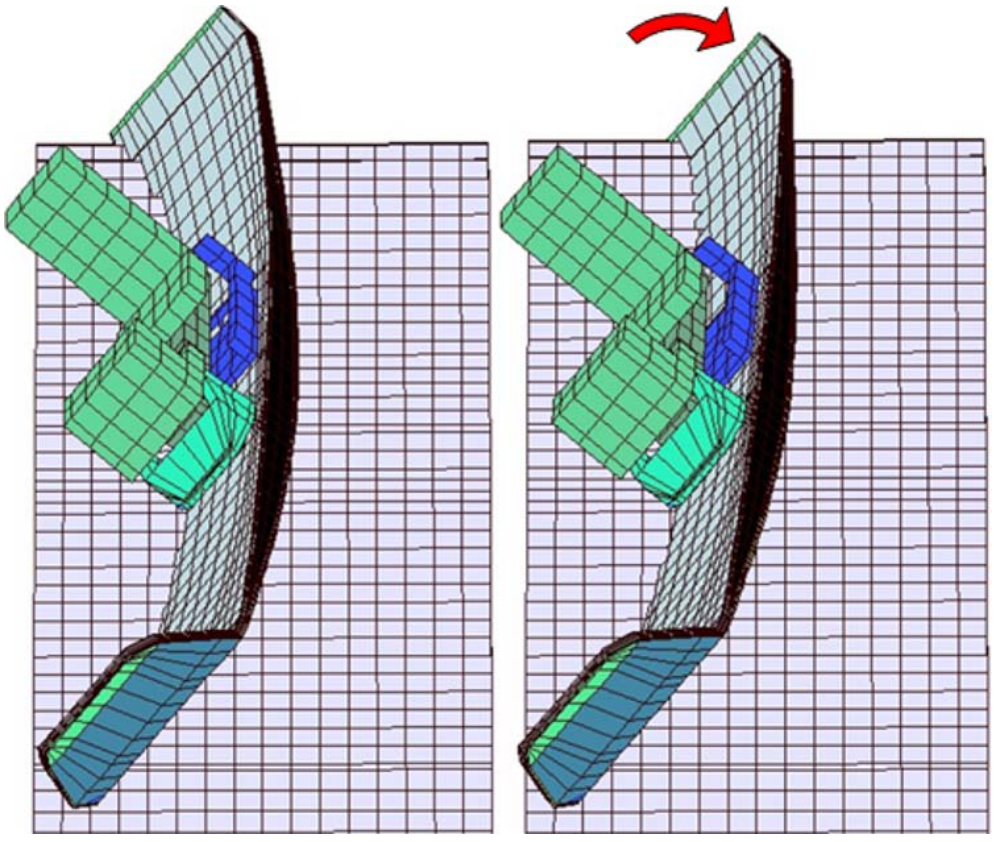

Fig. 3 Solution of the simulation for a static case (*left*) and for the case of a moving ski (*right*). The rotation of the ski's rear section into the groove is indicated. For better comparison the position of the snow surface is indicated by an additional mesh

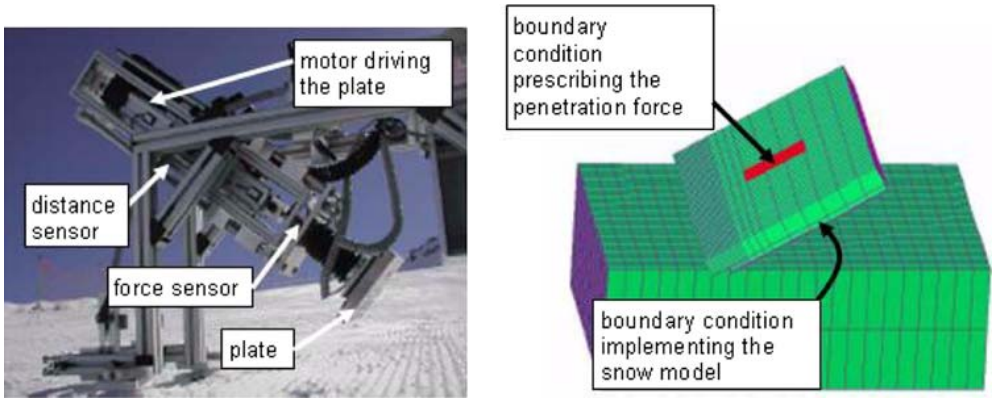

Fig. 4 Device used to measure snow resistive force on a plate pushed into the snow (*left*). Simulation of the plate pushed into the snow with the snow model as boundary condition on the bottom surface of the plate (*right*) ([27], modified)

motion and the skis' motion were captured with a video system (Redlake, San Diego, CA, USA). The kinematic data were analysed using WINanalyse software (Micromak Service, Berlin, Germany). This allowed determination of the edging angles and inertia forces in the reference system of the ski. The coefficients characterising the snow strength in the snow model were measured at several locations on the slope. The data from the video analysis, the dynamometers, and the snow measurements provided all input variables necessary for the simulation [27].

For the validation of the simulation results, the actual turn radius was determined (a) from the video analysis (which can be synchronised with the measurements providing the input data for the simulation), and (b) from the traces of the skis in the snow (geometer measurement with an accuracy in the millimetre range). Both datasets were used to determine the actual turn radius as a function of the position on the slope. The actual turn radius determined from the skis' traces were compared to the radius of the rear section of the ski obtained in the simulation for the same loading conditions. This was done in two steps: first the results of the static simulation were assessed, and then the results of the simulation incorporating the plasticity of the snow deformation and the sidecut effect were compared to the measured instantaneous turn radius.

Fig. 5 Static validation experiment to determine the ski deformation of an edged ski pressed into a snow surface [27]

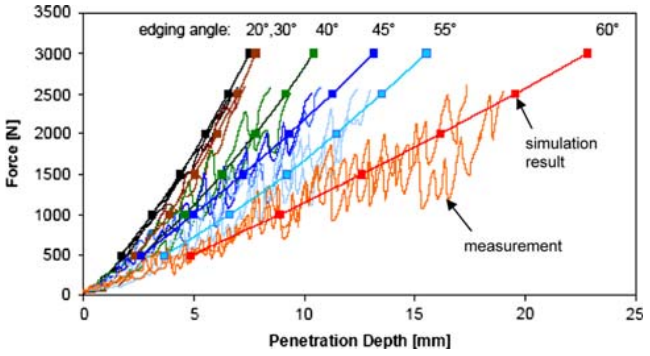

Fig. 6 Measured and simulated snow resistance force in function of the penetration depth for six different edging angles (hard snow on a racing slope)

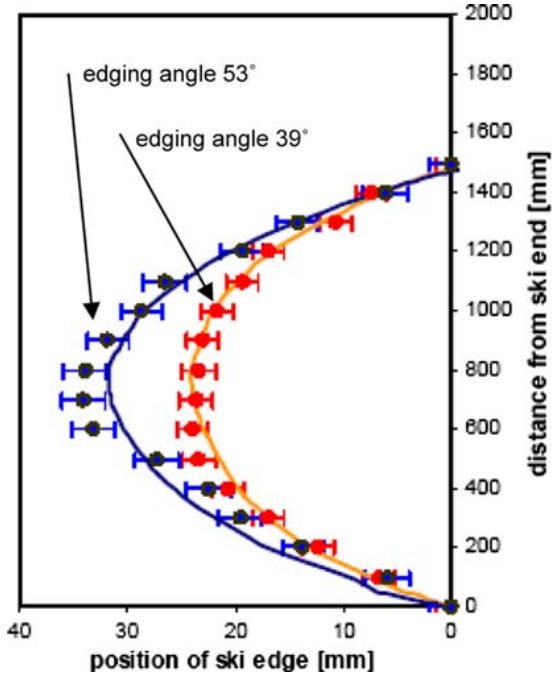

Fig. 7 Measured (*filled circle*) and simulated (*line*) positions of the ski edge projected to the snow surface for edging angles of 39 and 53° and a loading force of 3,000 N. The results are shown relative to an arbitrary line from ski end to shovel (*y* axis)

4 Results

4.1 Validation of the implemented snow model

For small edging angles (20°, 30°) the simulation calculated the same penetration depths for a given force as measured in the experiments (Fig. 6). For edging angles larger than 40° significant fluctuations around the general trend in the force–penetration depth measurements were observed. These fluctuations could be attributed to fracture processes within the snow taking place during the penetration. With the implemented snow model the simulation predicted the general trend in the force–penetration depth relationship, but did not account for fracture processes occurring within the snow.

4.2 Validation of the simulation result in a static case

The calculated and measured shapes of the lower ski edge projected on the plane of the snow surface are shown in Fig. 7 for edging angles of 39° and 53°. The general magnitude of the ski deflection was predicted correctly by the simulation. However, some differences between measurement and simulation results can be observed in the rear section of the ski (at distances between 200 and 800 mm from the ski end). The most likely explanation of these differences is that snow clods of varying size broke away during the experiment at some sections of the ski (visible in the photograph in Fig. 5). This created an inhomogeneous snow reaction and affected the shape of the ski.

4.3 Validation of the simulation result for a moving ski

The instantaneous turn radii calculated for the trace of the skis in the validation experiment revealed three

sections: an initiation phase, a drift phase, and the steering phase (Fig. 8a). The observed drift phase is typical for a modern ski racing technique and can be observed even in World-Cup ski races. The turn radius calculated in the simulation can be compared with the measured instantaneous radius in the initiation phase and in the steering phase of the turn, because the shape of the groove that remained in the snow indicated that in these phases the skis carved with no significant drifting or skidding.

In the static simulation only the results for the right ski, the inside ski in the turn, agree with the measured radius values (Fig. 8b). The results for the left ski, the outside ski, which is loaded with higher forces and generally more important for the turn, are significantly smaller (between 30 and 70%) than the measured instantaneous turn radii.

When the plasticity of the snow deformation and the side-cut effect are incorporated in the simulation, then the results for both skis agree well with the measured instantaneous turn radii (Fig. 8c). However, due to the modified boundary condition at the ski snow interface the simulation often does not converge to a reliable solution, particularly during the steering phase, when the edging angle of the ski exceeds 60°, the simulation did not converge to a valid solution.

5 Discussion

The validation of the snow model and of the ski in a quasi-static experiment shows that the simulation is in general able to calculate the correct penetration depth into the snow and the correct deformation of the ski in a quasi-static test. Small differences between simulation and measurement are caused by frequent fracture processes taking place in the snow. These processes occur more frequently at large edging angles and may indicate inhomogeneities in the snow fracture strength. Compared to other models used to estimate or calculate the turn radius of a ski, e.g. Howe's model [3], the static simulation presented here has the advantage that all of the important influencing variables are taken into account and their influence on the ski deformation or the ski–snow interaction can be studied. These influencing factors are the force and moment applied to the binding, the snow type, and the shape and composition of the ski.

The validation using the trace of an actual carved turn showed that a quasi-static approach to predict the turn radius of a ski is not applicable for a moving ski. Neither the quasi-static simulation presented here nor the model proposed by Howe were able to predict the instantaneous turn radius measured in the experiment. This suggests that purely quasi-static approaches to calculate the turn radius

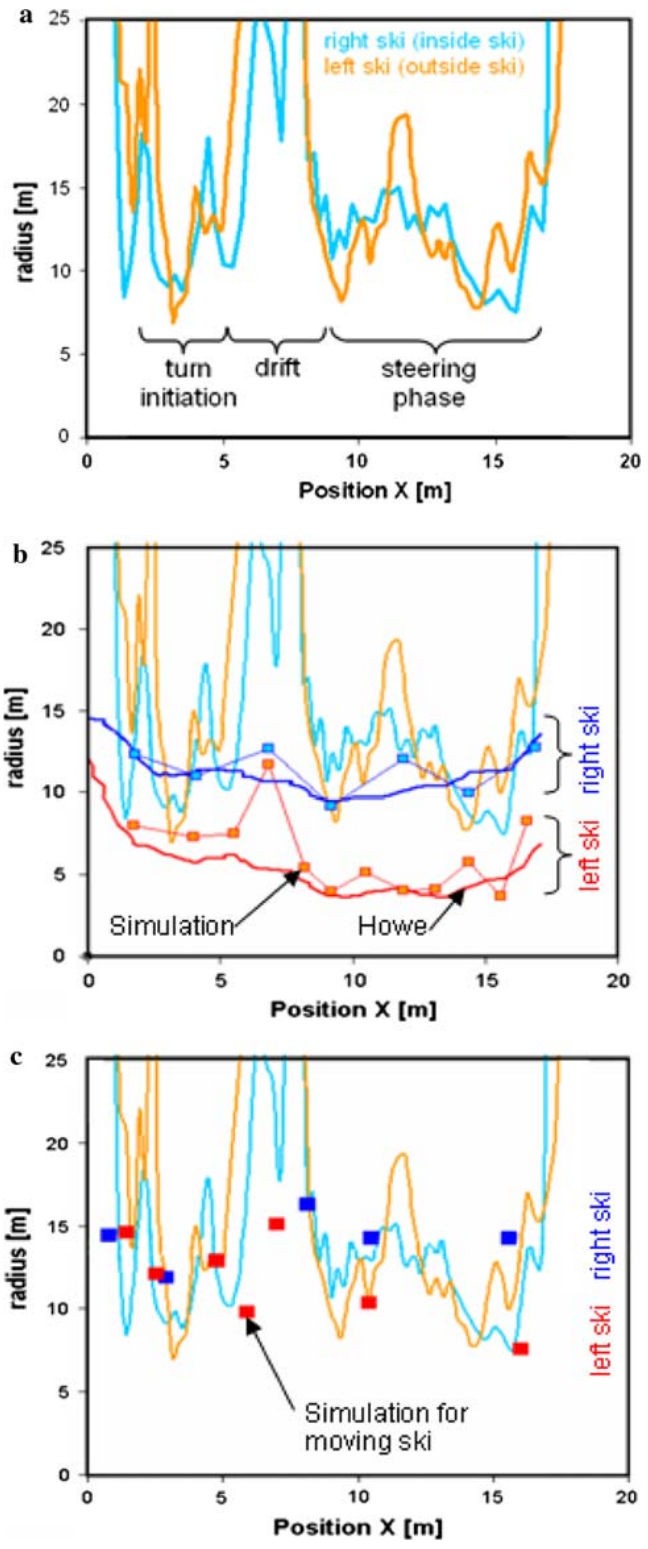

Fig. 8 **a** Measured instantaneous turn radii determined for both skis in the validation turn displayed as a function of the position along the fall line on the slope. **b** Comparison of measured instantaneous radii with turn radius calculated in the static simulation (*squares*) and with the prediction by Howe's model (*line*). **c** Comparison of measured instantaneous turn radii with turn radius calculated in the simulation incorporating plasticity of snow deformation and side-cut effect (*squares*)

or the deformation of a ski [33–35] that are based on Howe's model might need to be reconsidered.

The instantaneous radius of an actual carved turn was only predicted in a correct order of magnitude if two dynamic processes affecting the formation of the groove in the snow were taken into account. These processes are the plasticity of the snow deformation and effects of the side-cut on the shape of the groove. The former effect obviously takes place in the ski–snow interaction and does not need to be discussed further. The latter effect can be confirmed by examining the shape of the groove remaining in the snow after a carved turn [36] due to the side-cut and the ski's motion the angle of the groove is not 90° (as in a static case), but is typically about 120° (depending on the side-cut of the ski that created the groove). A consequence of this effect is that in a carved turn the curvature at the rear section of the ski is less than that of the front section. The radius of the rear section that glides through the groove is therefore larger than the radius of the front section forming the groove or the radius of the entire ski. Thus, the side-cut effect might offer an explanation for discrepancies reported in earlier studies, for example, Yoneyama et al. equipped a test ski with sensors that measured the ski deflection during an actual turn [37]. They reported (p. 12) that in the carving turns the "effective radius" determined from the deflection of the test ski was approximately 10 m, whereas the estimated radius of the skis' path was 20 m.

The incorporation of the dynamic effects in the simulation presented here allowed calculation of turn radii that agreed with radii determined from the skis' traces. For steady-state conditions the simulation thus allows calculation of reliable turn radii, ski deformation, or snow pressure profiles. The model can now be used to assess how varying input parameters, e.g. load on the binding, edging angles, snow conditions, ski composition or designs affect the turn radius or the ski–snow interaction (to be covered in a subsequent paper).

However, the simulation still has a number of significant limitations: (1) it only describes carved turns with no significant lateral skidding or drifting; (2) poor numerical stability due to the changing boundary conditions; (3) several necessary assumptions limit the applicability of the model. The most important restrictions are: (a) steady-state behaviour has to be assumed. Rapid changes of input variables e.g. the edging angle, would affect the actual ski deformation but will not affect the simulation result; (b) no moments may act on the binding, e.g. due to forward or backward leaning of the skier; (c) vibrations of the ski-binding system are not considered in this simulation model. In actual carved turns not only significant moments on the binding occur [27], but also significant vibrations in a bending mode were observed [38, 39]. The application of our model to predict actual carved turns is therefore still problematic.

A first step to overcome the limitations present in our model is the dynamic approach presented by Mössner et al. [28], who reported good agreement with sled measurements that create a steady-state turn. To overcome the condition that the ski has to be in a steady state, a dynamic simulation that includes a calculation of how the groove in the snow is formed would be necessary. Finite element simulations using modified Drucker–Prager or crushable foam element types might offer a means to realistically model the snow deformation [40, 41]. The most challenging issue to solve will be the huge number of elements that would be required to model the ski–snow interaction and the formation of the groove: the actual snow deformation occurs on a scale of a few centimetres or millimetres, which requires a high resolution of the finite element lattice representing the snow, while for a simulation of a full turn a spatial range of about 20 m would be required.

6 Conclusion and future work

Our and other models of the ski–snow interaction contribute to a better understanding of the physical processes governing skiing. In steady-state situations the turn radii, ski deformations, and snow pressure distributions can now be predicted. However, it is still a major challenge to link these results with performance or comfort characteristics of skis. Researchers and ski manufacturers who want to improve skiing equipment by using simulation approaches instead of the time consuming and expensive trial and error cycles need to address this lack of knowledge.

Acknowledgments The study was financially supported by the Swiss Foundation for Innovation KTI and the companies Stöckli Swiss Sports AG and Fritschi Swiss Bindings.

References

1. Casolo F, Lorenzi V (2001) Science and skiing II. In: Müller E, Schwameder H, Raschner C, Lindinger S, Kornexl E (eds) Relevance of ski mechanical and geometrical properties in carving technique: a dynamic simulation. Verlag Dr. Kovac, Hamburg, pp 165–179
2. Glenne B, DeRocco A, Vandergrift J (1997) The modern alpine ski. Cold Reg Sci Technol 26:35–38
3. Howe J (2001) The new skiing mechanics. McIntire Publishing, Waterford
4. Abele G, Gow AJ (1976) Compressibility characteristics of compacted snow. CRREL Rep
5. Federolf P, Fauve M, Szabó D, Lüthi A, Rhyner HU, Schneebeli M, Ammann W, Dual J (2004) Mechanical properties of snow during rapid impact. Snow Eng V:209–214

6. Mössner M, Nachbauer W, Innerhofer N, Schretter H (2003) Mechanical properties of snow on ski slopes. In: Abstract book of the 15th international congress on ski trauma and skiing safety, St. Moritz Switzerland
7. Lieu DK, Mote CD (1984) Experiments in the machining of ice at negative rake angles, J. Glaciology 30:77–81
8. Tada N, Hirano Y (2002) Search of the mechanics of a turning alpine ski using snow cutting force measurements. Sports Eng 5:15–22
9. Brown CA (2009) Modeling edge-snow interactions using machining theory. In: Müller E, Lindinger S, Stöggl T (eds) Science and skiing, vol IV. Meyer & Meyer Sport (UK) Ltd., pp 175–183
10. Colbeck SC (1988) The kinetic friction of snow. J Glaciol 34:78–86
11. Colbeck SC (1994) A review of the friction of snow skis. J Sports Sci 12:285–295
12. Outwater JO (1970) On the friction of skis. Med Sci Sports 2:231–234
13. Buhl D, Fauve M, Rhyner H (2001) The kinetic friction of polyethylene on snow: The influence of the snow temperature and the load. Cold Reg Sci Technol 33:133–140
14. Theile T, Szabo D, Luthi A, Rhyner H, Schneebeli M (2009) Mechanics of the ski–snow contact. Tribol Lett 36:223–231
15. Nigg BM, Neukomm PA, Spirig J, Unold E (1975) Vibration measurements during skiing, gymnastics, walking and running. Medizinische Welt 26:765–770
16. Fischer C, Overney LS, Fauve M, Blanke O, Rhyner H, Herzog MH, Bourban P, Månson J-E (2007) What static and dynamic properties should slalom skis possess? Judgements by advanced and expert skiers. J Sports Sci 25:1567–1576
17. Bruck F, Lugner P, Schretter H (2003) A dynamic model for the performance of carving skis. ASTM special technical publication, pp 10–23
18. Casolo F, Lorenzi, V, Vallatta, A, Zappa B (1997) Simulation techniques applied to skiing mechanics. In: Müller E, Schwameder H, Kornexl E, Raschner C (eds) Science and skiing. Taylor & Francis, pp 116–130
19. Clerc C, Gaertner R, Trompette P (1989) Computer aided design of skis. Finite Elem Anal Des 5:1–14
20. Hirano Y, Tada N (1996) Numerical simulation of a turning alpine ski during recreational skiing. Med Sci Sports Exerc 28:1209–1213
21. Kaps P, Mössner M, Nachbauer W, Stenberg R (2000) Pressure distribution under a ski during carved turns. In: Proceedings of the 2nd international congress on skiing and science, pp 180–202
22. Piziali RL, Mote Jr. CD (1972) Snow ski as a dynamic system. ASME J Dyn Syst Meas Control Ser G 94:133–138
23. Renshaw AA, Mote CD Jr (1989) A model for the turning snow ski. Int J Mech Sci 31:721–736
24. Nordt AA, Springer GS, Kollár LP (1999) Simulation of a turn on alpine skis. Sports Eng 2:181–199
25. Tada N, Hirano Y (1999) Simulation of a turning ski using ice cutting data. Sports Eng 2:55–64
26. Mössner M, Heinrich D, Kaps P, Schretter H, Nachbauer W (2009) Computer simulation of consecutive ski turns. ASTM Special Technical Publication 1510 STP, pp 126–136
27. Federolf P (2005) Finite element simulation of a carving snow ski. Pro BUSINESS GmbH, Berlin
28. Mössner M, Heinrich D, Schindelwig K, Kaps P, Lugner P, Schmiedmayer H, Schretter H, Nachbauer W (2006) Modeling of the ski–snow contact for a carved turn. In: Moritz EF, Haake S (eds) The engineering of sport, vol 6. Springer, New York, pp 195–200
29. Numerical Modeling GmbH (2003) NM-SESES, Finite element software for computer aided engineering. Numerical Modeling GmbH. Winterthur, Switzerland
30. Graber C (1990) Nichtlineare Analyse von Schalen mit linearisierten elastoplastischen Schnittkraft-Verformungs-Beziehungen. Verlag der Fachvereine, Zurich, Switzerland
31. Wäckerlin J (1997) Numerische Modellierung von Rennskis.Thesis, Zurich University of Applied Sciences
32. Federolf P, JeanRichard F, Fauve M, Lüthi A, Rhyner H, Dual J (2006) Deformation of snow during a carved ski turn. Cold Reg Sci Technol 46:69–77
33. Müller E, Schwameder H (2003) Biomechanical aspects of new techniques in alpine skiing and ski-jumping. J Sports Sci 21:679–692
34. Jentschura UD, Fahrbach F (2004) Physics of skiing: the ideal-carving equation and its applications. Can J Phys 82:249–261
35. Lind D, Sanders SP (1996) The physics of skiing. Springer-Verlag New York Inc., New York
36. Tatsuno D, Yoneyama T, Kagawa H, Scott N, Osada K. (2009) Measurement of ski deflection and ski–snow contacting pressure in an actual ski turn on the snow surface. In: Müller E, Lindinger S, Stöggl T (eds): Science and Skiing vol IV. Meyer & Meyer Sport (UK) Ltd
37. Yoneyama T, Scott N, Kagawa H, Osada K (2008) Ski deflection measurement during skiing and estimation of ski direction and edge angle. Sports Engineering 11:3–10
38. Scott N, Yoneyama T, Kagawa H, Osada K (2007) Measurement of ski snow-pressure profiles. Sports Eng 10: 145–156
39. Glenne B, DeRocco A, Foss G (1999) Ski and snowboard vibration. Sound Vib 33:30–33
40. Ghoreishy MHR (2008) A state of the art review of the finite element modelling of rolling tyres. Ir Polym J (English Edition) 17:571–597
41. Shoop S, Kestler K, Haehnel R (2006) Finite element modeling of tires on snow. Tire Science and Technology 34:2–37